



A Velocity Map Imaging Study of the Reactions of O^+ (4S) With CH_4

Linsen Pei and James M. Farrar*

Department of Chemistry, University of Rochester, Rochester, NY, United States

We present a velocity map imaging study of the key ion-molecule reactions occurring in the $O^+(^4S_{3/2}) + CH_4$ (X^1A_1) system at collision energies of 1.84 and 2.14 eV. In addition to charge transfer to form CH_4^+ (X^2B_2), we also present data on formation of CH_3^+ (X^1A_1'), for which the experimentally determined images provide clear confirmation that the products arise from dissociative charge transfer rather than hydride transfer. Experimental data are also presented on the formation of HCO^+ through a transient $[OCH_4]^+$ complex living many rotational periods. Plausible reaction pathways and intermediate structures are presented to give insight into the routes for formation of these reaction products.

OPEN ACCESS

Edited by:

Antonio Aguilar,
University of Barcelona, Spain

Reviewed by:

Daniela Ascenzi,
University of Trento, Italy
Peter B. Armentrout,
The University of Utah, United States

*Correspondence:

James M. Farrar
james.farrar@rochester.edu

Specialty section:

This article was submitted to
Physical Chemistry and Chemical
Physics,
a section of the journal
Frontiers in Chemistry

Received: 16 February 2019

Accepted: 22 March 2019

Published: 12 April 2019

Citation:

Pei L and Farrar JM (2019) A Velocity
Map Imaging Study of the Reactions
of O^+ (4S) With CH_4 .
Front. Chem. 7:227.
doi: 10.3389/fchem.2019.00227

Keywords: ion-molecule, potential energy surface, atmospheric chemistry, methane, oxygen ion

INTRODUCTION

The reactions of the oxygen cation with methane and other small hydrocarbons at hyperthermal energies have received significant experimental and theoretical attention in the past 10 to 15 years. That interest has been motivated in large part by understanding the chemistry taking place in many environments, chief among them planetary atmospheres and interstellar clouds (Wakelam et al., 2012). The role that ions play in eroding the surfaces of spacecraft in low-earth orbit has also been a question addressed by these studies (Levandier et al., 2004). The relative simplicity of such reactions has stimulated theoretical studies that have led to fruitful comparisons with experiment, especially for the methane system, as exemplified by the pioneering experimental and theoretical study of the reactions in the $O^+(^4S) + CH_4$ system by Levandier et al. (2004). Experimentally, this study employed the guided ion beam method to yield absolute cross sections as a function of collision energy for charge transfer, dissociative charge transfer and/or hydride abstraction, and carbon-oxygen bond formation. The overwhelmingly favored product for ground state O^+ reactants was charge transfer to produce CH_4^+ . Theoretically, the study employed *ab initio* electronic structure calculations of quartet and doublet potential energy surfaces for the $(O \bullet CH_4)^+$ species that provided qualitative interpretations for the dominant reactive pathways.

More recent experiments by Cunha de Miranda et al. (2015) have focused on reactivity in the ground quartet (4S) and first two excited doublet (2D and 2P) states. Electronically state-selected reactant O^+ ions were prepared by dissociative ionization of O_2 using VUV photons from the DESIRS beamline. Like the experiments of Levandier et al., this study has employed guided beam methodology to determine absolute cross sections and branching ratios over an extended collision energy range from thermal to several eV. These experiments confirm that the dominant products

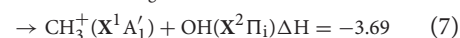
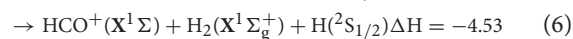
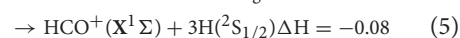
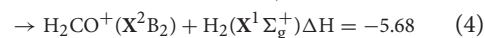
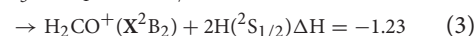
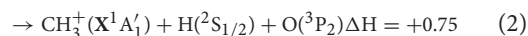
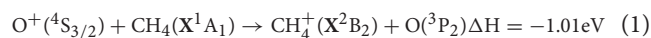
for ground and excited state O⁺ reactants are CH₄⁺ and CH₃⁺, but with branching ratios that have a strong electronic state dependence. For ground state O⁺ reactants, the experimental data confirm the results of Levandier et al. that the CH₄⁺ charge transfer product is overwhelmingly favored. However, electronic excitation to the ²D and ²S states of O⁺ results in a strong preference for CH₃⁺ production. The authors did not report data for the products from C-O bond formation.

Both the experiments of Cunha de Miranda et al. and Levandier et al. make inferences about product energy and angular distributions from guided ion beam data taken at fixed collision energies. Under normal guided beam operation, the amplitude of the radiofrequency (rf) trapping voltage is sufficiently large to transmit all ions irrespective of the relative magnitudes of the longitudinal or transverse components of product velocities. In this mode of operation, measurements of the time-of-flight distributions for individual products yield projections of their speed distributions along the relative velocity vector. Additional experiments in which the rf amplitude is reduced significantly decrease the trapping well depth, allowing products with significant transverse velocities to escape detection. Such experiments yield more sensitive determinations of the forward and backward scattered product intensities, for which the latter are especially diagnostic of resonant charge transfer.

These experiments, along with computations that provide details of the potential energy surfaces, reactive intermediates and their structures, and related trajectory studies (Sun and Schatz, 2005) have answered a number of questions about the formation of the primary CH₄⁺ and CH₃⁺ products, as well as C-O bond formation, especially for ground state O⁺(⁴S). However, experimental limitations of the guided ion beam method have left open questions about whether CH₃⁺ is formed simply by dissociative charge transfer on the ground quartet state surface, or whether intersystem crossing to the doublet manifold facilitates hydride transfer to provide an additional route for CH₃⁺ production. In contrast to the ground quartet state of O⁺, each of the excited doublet states of O⁺ has a vacant *2p* orbital that can accept an electron pair from the hydride ion H⁻. Furthermore, existing evidence showing that formation of the H₂CO⁺ and HCO⁺ products occurs through a long-lived complex is suggestive, but not robust. In the present study, complete velocity space flux distributions obtained by the velocity map imaging (VMI) method provide the robust evidence necessary to clarify the mechanisms of these important reaction channels.

The objective of the experiments reported here is to clarify the mechanism by which CH₃⁺ is formed, and to provide deeper insight into the production of HCO⁺ by C-O bond formation. Velocity space images of these products, along with data for the charge transfer process, are offered in support of the claim that the methyl cation, CH₃⁺, is produced by dissociative charge transfer on the ground quartet surface via reaction (2) shown below, rather than hydride abstraction via reaction (7), and that the products H₂CO⁺ and HCO⁺ appear to be formed by a spin-allowed condensation mechanism in the quartet manifold

of potential surfaces. The observed reactions and their energetics are listed below:



Reaction energetics are taken from Table 1 of Sun and Schatz and Table 3 of Levandier et al.

EXPERIMENTAL

As described previously (Pei and Farrar, 2012), the experiment is conducted with a crossed beam instrument employing velocity map product imaging (VMI) detection (Eppink and Parker, 1997). The imaging system determines all product velocities for a given mass in a single detection time window, yielding significant enhancement of detection efficiency through the intrinsic multiplex advantage of the method. Our implementation of VMI is based upon important developments from other laboratories (Reichert et al., 2000, 2002; Reichert and Weisshaar, 2002; Mikosch et al., 2006, 2008; Zhang et al., 2010).

The primary ion beam is formed by electron impact (Udseth et al., 1973) on a mixture of 10% CO in He. The primary product of electron impact on this mixture is He⁺, which then undergoes charge transfer with CO to form both parent and fragment C⁺ and O⁺ cations. The electronic state distribution of O⁺ produced in this manner can be assessed by using observations by Smith et al. (1992) which showed that charge transfer between O⁺ and CO is endoergic for ground state cations, but is exoergic for the ²S and ²D excited states. In a crossed beam geometry in which the O⁺ ion beam intersected a CO beam, we were unable to detect CO⁺ cations. This observation places a limit on excited state O⁺(²D, ²P) production of less than 1%.

In our experiment, the O⁺(⁴S) ions produced by electron impact are extracted, mass selected, and decelerated and focused by a series of ion optics, and the continuous beam of ions is delivered to the volume defined by the repeller and extraction electrodes of a VMI detector. The ion beam has a roughly triangular kinetic energy distribution with a FWHM of approximately 0.20 eV in the laboratory frame of reference.

The neutral beam is a supersonic expansion produced by a pulsed solenoid valve located 10 mm upstream from a 1 mm skimmer. The stagnation pressure of the CH₄ gas behind the 0.1 mm diameter nozzle is 3 atm, and the resulting velocity distribution has a FWHM of ~6–8%. The pressure in the collision chamber is ~3 × 10⁻⁷ torr with the beams running.

Under the experimental conditions, the relative velocity of the reactants at a collision energy of 1.84 eV is 6,620 m/s. At E_{col} = 2.14 eV, the relative velocity of approaching reactants is 7,140 m/s.

The reactant beams intersect at the center of a collision volume defined by two circular electrodes of radius 38 mm spaced by 20 mm. The lower, repeller electrode and the upper, extractor electrode are held at ground potential as the ion and neutral beams intersect. Product detection is achieved by velocity map imaging (Eppink and Parker, 1997) with the two-electrode geometry described by the Suits research group (Townsend et al., 2003). Product detection is initiated by pulsed electric fields applied to the collision volume after reaction has taken place. The detection pulses, applied with separate high voltage pulse generators (DEI PVX-4140, 4150), are synchronized to the arrival of the central portion of the pulsed molecular beam and have a rise time and duration of 25 ns and 1 to 2 μ s, respectively to allow all products to escape the volume between the repeller and extractor within the pulse duration.

Delayed pulsed extraction is achieved by pulsing the voltage on the repeller plate, V_1 , to +2300 V, the precise value dependent on transverse velocity and the filling factor for the MCP detector. The voltage V_2 on the 13 mm aperture extraction electrode is pulsed to a value $V_2 = 0.65 V_1$. A grounded electrode with a 20 mm aperture placed 13 mm above the extraction electrode provides velocity mapping for the product ions at the imaging plane, located 0.6 m downstream from the grounded lens.

Prior to striking the imaging plane of the detector, defined by the front face of a pair of chevron-mounted microchannel plates, the ions pass through a grounded grid. The MCPs are gated by a pulse of base width 80 ns, which results in an effective “on” time of ~ 40 ns, during which the product ion cloud is recorded by the phosphor screen following the MCP anode. Under these operating conditions, the three-dimensional ion cloud is effectively “crushed” as it reaches the MCP detection plane.

The light image from the phosphor screen is recorded by a CCD camera (uEye 2230), which transfers the image via a USB interface to a lab computer controlled by LabView software. A typical image represents the accumulation of 5,000 to 20,000 repetitions of the pulsed valve.

RESULTS AND DISCUSSION

Velocity space images were collected for the CH_4^+ , CH_3^+ , and HCO^+ products at collision energies 1.84 and 2.14 eV. Images for CH_2^+ and H_2CO^+ formation were also detected. Because of the very strong similarities of these images to those for CH_3^+ and HCO^+ , respectively, we have not shown them in this paper. Branching fractions for all five observed products are reported in **Table 1** and are compared with the results of Cunha de Miranda et al.

Figure 1 shows product images for charge transfer to form CH_4^+ , dissociative charge transfer and/or hydride transfer forming CH_3^+ , and C-O bond formation to form HCO^+ . The left column shows products formed at 1.84 eV and the right column shows the corresponding images at 2.14 eV. The dominant products correspond to CH_4^+ and CH_3^+ formation, with comparable intensities at both collision energies, as **Table 1** shows. These results are consistent with those of Cunha de Marino et al., although the relative yield of CH_3^+ is higher in our experiments. Secondary collisions occurring in the experiments with state-selected ions may be responsible for the differences

TABLE 1 | Product branching ratios.

Product	$E_{\text{rel}} = 1.84 \text{ eV}$		$E_{\text{rel}} = 2.14 \text{ eV}$	
	Fraction		Fraction	
CH_4^+	0.44 ± 0.09^a	$(0.83)^b$	0.47 ± 0.09^a	$(0.83)^b$
CH_3^+	0.49 ± 0.09^a	$(0.15)^b$	0.46 ± 0.09^a	$(0.15)^b$
CH_2^+	0.06 ± 0.02^a	$(0.02)^b$	0.05 ± 0.02^a	$(0.02)^b$
H_2CO^+	0.005 ± 0.003^a		0.005 ± 0.003^a	
HCO^+	0.008 ± 0.004^a		0.01 ± 0.004^a	

^aThis work.

^bCunha de Miranda et al. (2015).

in branching fractions. Images for H_2CO^+ production are very similar to those for HCO^+ formation, and are not reported here.

The planar MCP detection system recovers images as product ion flux in Cartesian coordinates, either in the laboratory (v_x , v_y) or in the center of mass frame (u_x , u_y). Transformation of lab velocity (v_x , v_y) to center of mass velocity (u_x , u_y) is accomplished by a simple velocity shift **C** describing the motion of the center of mass of the collision system:

$$\mathbf{u} = \mathbf{v} - \mathbf{C} \quad (8)$$

Because the volume elements in both representations are equal, i.e., $dv_x dv_y = du_x du_y$, (Wolfgang and Cross, 1969; Friedrich and Herman, 1984), center of mass flux $P(u_x, u_y)$ may be visualized directly from the measured image. The full three-dimensional image and thus kinetic energy and angular distributions may be extracted from the experimental images by application of the BASEX algorithm (Dribinski et al., 2002). We do not report those distributions in this paper.

CH_4^+ Formation

At both collision energies, the CH_4^+ charge transfer products, shown in the top panel of **Figure 1**, appear near the velocity of the incident CH_4 reactant, consistent with energy resonance, with minimal conversion of reactant kinetic energy into product internal excitation. The circles shown on the images define the maximum kinetic energies accessible to the products, assuming that the total energy of the products, given as the sum of incident kinetic energy and reaction exoergicity, appears as product translation.

This strong peaking of product velocity is consistent with minimal deflection of the CH_4 framework during electron transfer, and is consistent with large impact parameter collisions in which the electron is transferred to the ion at long range. The images show that the CH_4^+ speed distributions are very narrow, indicative of a very small number of populated CH_4^+ vibrational states. The energy widths of the CH_4^+ product distributions are $\sim 0.13 - 0.15 \text{ eV}$, or $1,000$ to $1,200 \text{ cm}^{-1}$.

From the perspective that charge transfer is driven not only by energy resonance, but also by the existence of favorable Franck-Condon (FC) factors between the reactant neutral and its corresponding ion, the narrow width suggests that the ionic potential energy surface is very steep in the FC region. However, the nature of the ionization process in CH_4 requires more detailed consideration. Because the geometries of CH_4 and CH_4^+

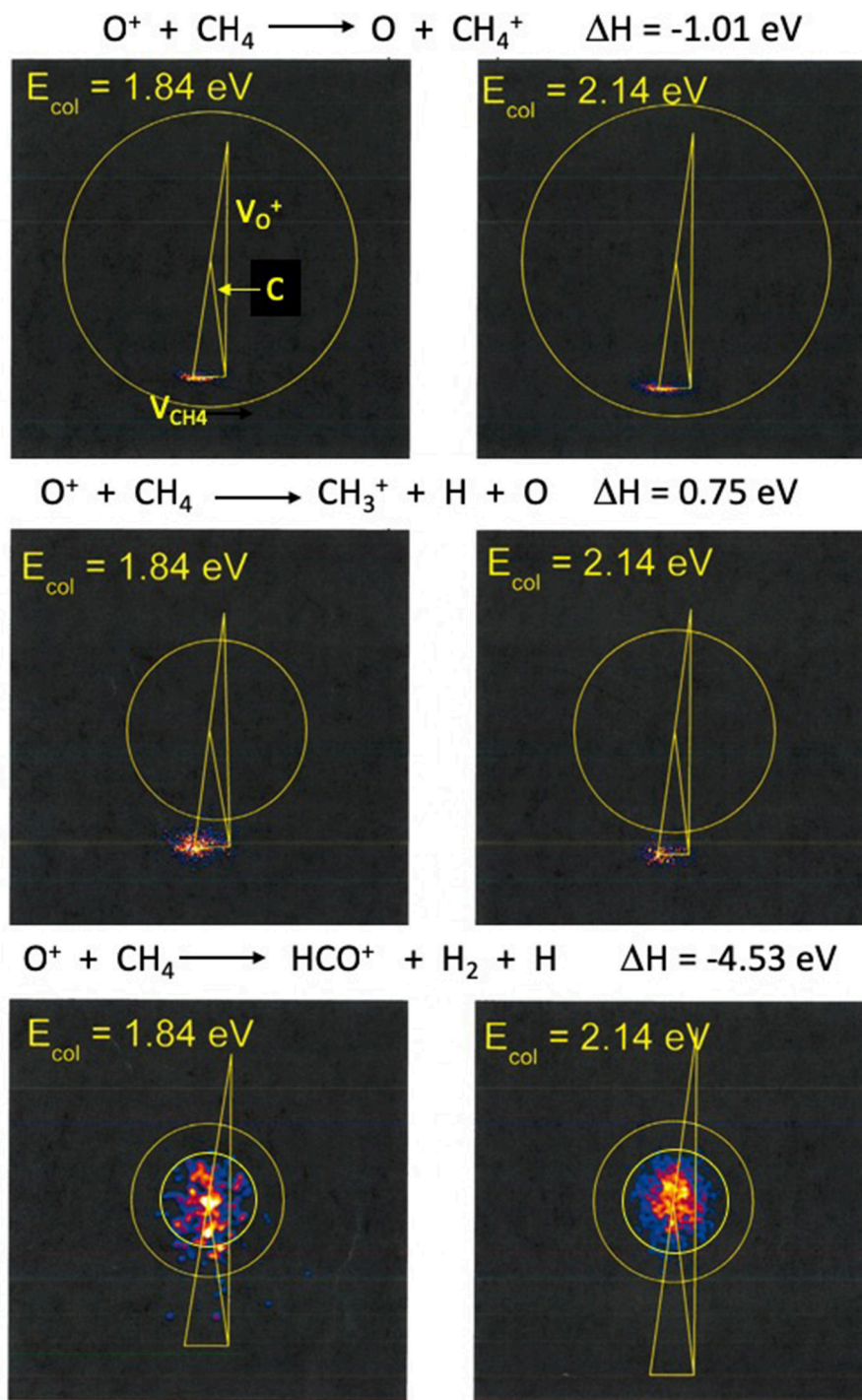


FIGURE 1 | Ion images for CH_4^+ , CH_3^+ , and HCO^+ production superimposed on the most probable Newton diagram. The directions of the O^+ and CH_4 beams are indicated on the top left image, and are not repeated on the other five frames to avoid cluttering the figure. The direction of the system center of mass is denoted by **C**. Laboratory velocities \mathbf{v} are measured from the beam intersection point, and center of mass velocities \mathbf{u} are measured relative to the tip of **C**. The left column of images corresponds to $E_{\text{rel}} = 1.84 \text{ eV}$, and the right column corresponds to $E_{\text{rel}} = 2.14 \text{ eV}$. Under the experimental conditions, the relative velocity of the reactants at a collision energy of 1.84 eV is 6,620 m/s. At $E_{\text{col}} = 2.14 \text{ eV}$ the relative velocity of approaching reactants is 7,140 m/s. The top row of images shows the formation of CH_4^+ by charge transfer, and the circle corresponds to the barycentric speed associated with the thermochemical limit for reaction (1). The middle row of images shows CH_3^+ produced by dissociative charge transfer, with the circle corresponding to the thermochemical limit for $\text{CH}_3^+ + \text{O} + \text{H}$, the atomic products formed with zero relative kinetic energy, reaction (2). The bottom row of images shows HCO^+ formation. The larger circle corresponds to maximum product speed allowed by energy conservation for the formation of $\text{HCO}^+ + \text{H}_2 + \text{H}$, reaction (6). The smaller circle corresponds to the maximum product speed allowed by energy conservation for the formation of $\text{HCO}^+ + \text{H} + \text{H} + \text{H}$, reaction (5).

are significantly different (Coulson and Strauss, 1962; Frost et al., 1967; Dixon, 1971), one expects that electron transfer, like photoabsorption, is constrained by the geometry change accompanying the process. Important early studies of charge transfer at thermal energies (Laudenslager et al., 1974) underscore the critical role of energy resonance and favorable Franck-Condon factors in determining reaction rates, but do not establish criteria that predict which effect is most important. In the present system, the charge transfer process requires crossings between potential surfaces that correspond asymptotically to (O⁺ + CH₄) and (O + CH₄⁺), and the collision dynamics in the vicinity of these crossings modulate the effect of favorable Franck-Condon factors. The high dimensionality of the surfaces makes a detailed quantum analysis of those crossings difficult, if not intractable.

CH₃⁺ Formation

The images for CH₃⁺ formation in the middle panels of **Figure 1** clearly resemble those for direct charge transfer, centered on the tip of the CH₄ neutral velocity vector. The images clearly lie outside the circles that define the locus of speeds consistent with three body collision-induced dissociation (CID). Those circles are defined by the maximum speed that a CH₃⁺ product would have when accompanied by an (O,H) pair bound with zero energy. The appearance of CH₃⁺ products outside those circles indicates that three-body CID is not the production mechanism for CH₃⁺. Rather, that product appears to originate from nascent CH₄⁺.

The energy resonance condition that governs the formation of CH₄⁺ imparts approximately 1.0 eV of internal energy to the ion. The kinetic energy contribution to the total energy available to the nascent CH₄⁺ arises from the initial kinetic energy less the kinetic energy removed by the oxygen atom also produced in the charge transfer process. Momentum conservation requires that the oxygen atom removes exactly half of the available kinetic energy, or ~0.9 to 1.1 eV. Thus, the total energy available to the nascent CH₄⁺ products of charge transfer ranges from 1.9 to ~2.1 eV. Reaction exoergicities show that the appearance potential for CH₃⁺ from CH₄⁺ is 1.84 eV. Considering the incident collision energy spread and the narrow but non-zero energy spread in the internal energy imparted to the nascent CH₄⁺ products, it is clear that a significant fraction of those products have sufficient energy to decay to CH₃⁺.

The methyl cation may also be formed by hydride transfer from CH₄ to O⁺, a process exoergic by 3.69 eV. Previous studies have shown that hydride transfer from a methyl carbon atom to O⁺ (Curtis and Farrar, 1986) and to CH₃⁺ ions (Zabka et al., 1995) results in kinetic energy release distributions that are significantly broader and peaked to higher energies than electron transfer to the same approaching ion. Moreover, the ground quartet electronic state of O⁺ does not contain an empty 2*p* orbital to accommodate an electron pair from the hydride group H⁻. Therefore, hydride transfer to O⁺ should be strongly suppressed relative to electron transfer owing to its spin-forbidden character, and its dynamics should be very distinct from those of charge transfer. Thus, strong evidence supports the claim that CH₃⁺ is formed by spin-allowed dissociative charge transfer, reaction (2), rather than spin-forbidden hydride transfer, reaction (7). This claim has also been advanced by Cunha de Miranda et al.

The images for CH₃⁺ formation are broadened relative to their CH₄⁺ precursor images. The kinetic energy widths for the parent ions correspond to ~0.13 to 0.15 eV, and the widths of the CH₃⁺ daughter ions are ~0.06 eV larger. This broadening corresponds to roughly 20 to 30% of the total energy in excess of the dissociation threshold for CH₄⁺ decay to CH₃⁺, a result consistent with statistical unimolecular decay theories (Marcus, 1952).

HCO⁺ Formation

The velocity space images for HCO⁺ formation are shown in the bottom row of images in **Figure 1**. Despite the kinematic constraint that the HCO⁺ products must appear close to the system center of mass in velocity space, the data are clear and precise, and allow the claim that HCO⁺ is distributed symmetrically in the center of mass frame and arises from decay of a long-lived precursor. The larger diameter circles shown in the images in the lowest row in **Figure 1** correspond to the maximum speeds the HCO⁺ + H₂ + H products could have if all available energy appears in translation. Similarly, the smaller circles correspond to the maximum speeds of HCO⁺ products formed along with three hydrogen atoms. At the lower collision energy, most of the flux falls within the smaller circle, suggesting that the spin-allowed pathway is the dominant one, and only a small fraction of the products are accompanied by molecular hydrogen formation. At the higher collision energy, all of the flux falls cleanly within the smaller circle.

The computations reported by Levandier et al. (2004) that consider reaction on both quartet and doublet potential surfaces, and by Sun and Schatz (2005), who focus only on quartet surfaces, provide a computational basis for understanding the reaction dynamics. The reaction coordinate schematic shown in **Figure 2** contains information extracted from those references. This pathway has been explored experimentally by Anderson et al. (Liu et al., 2005) and theoretically by Lorquet et al. (Pires et al., 1978), as well as in the work of Levandier et al. and Sun and Schatz.

As indicated in **Figure 2**, resonance charge transfer occurs on a quartet potential surface, and the nascent products O + CH₄⁺ lead to the important intermediate quartet complex denoted QCP1, as well as a doublet state complex labeled DCP1 in Levandier et al. and Sun and Schatz. In the complex QCP1, which lies 1.7 eV in energy below the O⁺ + CH₄ reactants, a hydrogen atom from the methyl cation serves as a bridge between the carbon and oxygen atoms. The transition state QTS1 leading to the H₂CO⁺ product has charge localized on the methane moiety, with significant spin density on the oxygen atom, and product cation is formed by ejection of two hydrogen atoms. This mechanism allows a doublet state ion to be formed in concert with two doublet state hydrogen atoms on a quartet state surface. The quartet surface shown in **Figure 2** has fairly shallow wells (1.0 eV for the charge transfer products and 1.7 eV for QCP1), has a barrier at QTS1 that lies 0.07 eV above the approaching reactants, and products at 1.23 eV below the reactants. Given the relatively sparse densities of vibrational states in QCP1 and QTS1, it is unlikely that QCP1 will have a lifetime long enough to exhibit the signature of a long-lived complex.

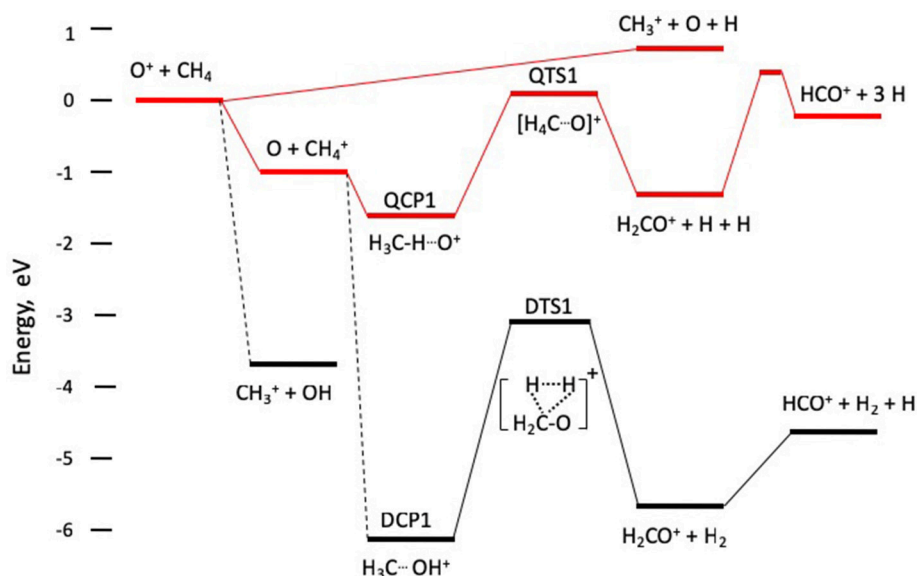


FIGURE 2 | Schematic reaction coordinate diagram for formation of CH_4^+ , CH_3^+ , and HCO^+ formation. The upper set of intermediates and transition states QCP1 and QTS1 evolving from $\text{O} + \text{CH}_4^+$ to $\text{H}_2\text{CO}^+ + \text{H} + \text{H}$ on the quartet potential surface, shown schematically in red. The lower set of intermediates and transition states DCP1 and DTS1 evolve from $\text{O} + \text{CH}_4^+$ to $\text{H}_2\text{CO}^+ + \text{H}_2$ on the doublet potential surface.

The doublet state complex DCP1 is not directly accessible from the quartet state charge transfer products, and the dotted line connecting them, discussed by Levandier et al. (2004), suggests that an internal conversion process accesses motion on surfaces in the doublet manifold. The complex DCP1 is formed by insertion of O into a C-H bond, leading to the incipient C-O bond in H_2CO^+ . Migration of a hydrogen atom from O to C leads to a three-center transition state, DTS1, lying ~ 3 eV above DCP1, that ejects molecular hydrogen in concert with the ground state formaldehyde cation, H_2CO^+ . Formation of HCO^+ over a barrier of ~ 0.6 eV is observed computationally, and Table 1 indicates that H_2CO^+ and HCO^+ have comparable intensities.

The formation of H_2CO^+ via QCP1 on the quartet surface is accompanied by two hydrogen atoms. In contrast, H_2CO^+ production via DCP1 on the doublet surface is accompanied by molecular H_2 formation. Thus, the total energies available to the quartet state products, the sum of collision energy and exoergicity for $\text{HCO}^+ + 3\text{H}$, are ~ 1.9 and 2.2 eV for the two collision energies respectively, while ~ 6.4 and 6.7 eV are accessible to the $\text{HCO}^+ + \text{H}_2 + \text{H}$ products formed on the doublet surface. At the lower (higher) collision energy, products formed with more than 1.9 (2.2) eV of translation must be assigned to formation on the doublet surface, while products formed with 1.9 (2.2) eV or less may be formed on either surface. Qualitative bounds on the kinetic energy release can be gleaned from the images in Figure 1, particularly at the higher collision energy. The data show clearly that kinetic energy release is fairly small, with most of the flux confined within the smaller of the two circles shown in each of the images in the bottom panel of Figure 1. Those smaller circles correspond to the maximum speeds accessible to $\text{HCO}^+ + 3\text{H}$ products. The images support the claim that a very small fraction of the products are formed following internal conversion to the doublet surface.

CONCLUSIONS

The experimental data reported here for CH_4^+ , CH_3^+ , and HCO^+ formed in the reactions of $\text{O}^+(^4\text{S})$ with CH_4 , in conjunction with reaction pathways proposed by Levandier et al. and Sun and Schatz, provide clear evidence that the primary CH_4^+ product is formed in a very narrow range of vibrational states by resonant charge transfer. The experimental data for CH_3^+ formation provide strong evidence that this product, formed with comparable cross section, arises from dissociation of nascent CH_4^+ on the quartet potential surface, rather than by the spin-forbidden process of hydride transfer.

Although HCO^+ production is a minor channel, formed at less than 1% of the total product yield, the pathways for its formation are quite interesting. The spin-allowed quartet surface pathway leads to formation of H_2CO^+ in conjunction with ejection of two hydrogen atoms. Unimolecular decay of the nascent H_2CO^+ product by C-H bond cleavage yields $\text{HCO}^+ + \text{H}$ with ~ 60 to 65% yield. Computations also suggest a viable pathway for H_2CO^+ production (with subsequent decay to HCO^+) in concert with an H_2 molecule via internal conversion from the lowest quartet state to the doublet manifold.

The experimental data show that the kinetic energy release for H_2CO^+ formation and subsequent decay to HCO^+ is quite low, ~ 2 eV or smaller. No products are formed with kinetic energies in the range between 2.2 and 6.7 eV, where energy conservation constrains products to be formed on the doublet surface. There is no experimental evidence to claim that any of the observed reaction products must be formed by spin-forbidden processes. Although one might expect that the tight transition state DTS1 preceding H_2 ejection would produce translationally excited products, the data provide no evidence for that expectation.

The experimental data presented here have demonstrated that ion imaging has yielded additional insights into the benchmark O⁺ + CH₄ system, complementing important contributions, both experimental and theoretical, already in the literature. We hope that imaging methods will continue to play an important role in elucidating the dynamics of prototypical systems in atmospheric chemistry and astrochemistry.

DATA AVAILABILITY

The datasets generated for this study are available on request to the corresponding author.

REFERENCES

- Coulson, C. A., and Strauss, H. L. (1962). Static Jahn-Teller distortions in small molecules CH₄⁺, CF₄⁺, NH₃⁺ (excited state) and NDNH₃ (excited state). *Proc. R. Soc. Lond. Ser. A* 269, 443–455. doi: 10.1098/rspa.1962.0188.
- Cunha de Miranda, B., Romanzin, C., Chefdiville, S., Vuitton, V., Žabka, J., Polásek, M., et al. (2015). Reactions of state-selected atomic oxygen ions O⁺(⁴S, ²D, ²P) with methane. *J. Phys. Chem. A* 19, 6082–6098. doi: 10.1021/jp512846v.
- Curtis, R. A., and Farrar, J. M. (1986). A low energy crossed beam study of the hydride abstraction and charge transfer reactions of C⁺ with CH₃OH. *Chem. Phys. Lett.* 123, 471–475. doi: 10.1016/0009-2614(86)80045-8
- Dixon, R. N. (1971). Jahn-Teller distortion of CH₄⁺. *Mol. Phys.* 20, 113–126. doi: 10.1080/00268977100100121.
- Dribinski, V., Ossadtchi, A., Mandelshtam, V. A., and Reisler, H. (2002). Reconstruction of Abel-transformable images: the gaussian basis-set expansion Abel transform method. *Rev. Sci. Instrum.* 73, 2634–2642. doi: 10.1063/1.1482156
- Eppink, A., and Parker, D. H. (1997). Velocity map imaging of ions and electrons using electrostatic lenses: application in photoelectron and photofragment ion imaging of molecular oxygen. *Rev. Sci. Instrum.* 68, 3477–3484. doi: 10.1063/1.114831
- Friedrich, B., and Herman, Z. (1984). Processing of ion-molecule beam scattering data: framework of scattering diagrams and derived quantities. *Collect. Czech. Chem. Commun.* 49, 570–585. doi: 10.1135/cccc19840570
- Frost, D. C., McDowell, C. A., and Vroom, D. A. (1967). Ionization potentials of ammonia. *Can. J. Chem.* 45, 1343–1345. doi: 10.1139/v67-221.
- Laudenschlager, J. B., Huntress, W. T., and Bowers, M. T. (1974). Near thermal energy charge transfer reactions of rare gas ions with diatomic and simple polyatomic molecules: the importance of Franck-Condon factors and energy resonance on the magnitude of the rate constants. *J. Chem. Phys.* 61, 4600–4617. doi: 10.1063/1.1681779
- Levandier, D. J., Chiu, Y. H., Dressler, R. A., Sun, L. P., and Schatz, G. C. (2004). Hyperthermal reactions of O⁺(⁴S_{3/2}) with CD₄ and CH₄: theory and experiment. *J. Phys. Chem. A* 108, 9794–9804. doi: 10.1021/jp047993y
- Liu, J., Van Deventer, B., and Anderson, S. L. (2005). Vibrational mode and collision energy effects on reaction of H₂CO⁺ with C₂H₂: charge state competition and the role of Franck-Condon factors in endoergic charge transfer. *J. Chem. Phys.* 123:204313. doi: 10.1063/1.2128670.
- Marcus, R. A. (1952). Unimolecular dissociations and free radical recombination reactions. *J. Chem. Phys.* 20, 359–364. doi: 10.1063/1.1700424
- Mikosch, J., Fruhling, U., Trippel, S., Schwalm, D., Weidemüller, M., and Wester, R. (2006). Velocity map imaging of ion-molecule reactive scattering: the Ar⁺ + N₂ charge transfer reaction. *Phys. Chem. Chem. Phys.* 8, 2990–2999. doi: 10.1039/b603109a
- Mikosch, J., Trippel, S., Eichhorn, C., Otto, R., Lourderaj, U., Zhang, J. X., et al. (2008). Imaging nucleophilic substitution dynamics. *Science* 319, 183–186. doi: 10.1126/science.1150238
- Pei, L., and Farrar, J. M. (2012). Imaging ion-molecule reactions: charge transfer and C-N bond formation in the C⁺ + NH₃ system. *J. Chem. Phys.* 136:204305. doi: 10.1063/1.4719808
- Pires, M. V., Galloy, C., and Lorquet, J. C. (1978). Unimolecular decay paths of electronically excited species. I. H₂CO⁺. *J. Chem. Phys.* 69, 3242–3249. doi: 10.1063/1.436974.
- Reichert, E. L., Thureau, G., and Weisshaar, J. C. (2002). Velocity map imaging of ion-molecule reaction products: Co⁺(³F₄) + isobutane. *J. Chem. Phys.* 117, 653–665. doi: 10.1063/1.1482369
- Reichert, E. L., and Weisshaar, J. C. (2002). Nonstatistical translational energy distribution of H₂ elimination products from Co⁺(³F₄) plus propane. *J. Phys. Chem. A* 106, 5563–5576. doi: 10.1021/jp0137827
- Reichert, E. L., Yi, S. S., and Weisshaar, J. C. (2000). Bimolecular ion-molecule collisions in real time: Co⁺(³F₄) plus n-butane and isobutane reactions. *In: J. Mass Spectrom.* 196, 55–69. doi: 10.1016/S1387-3806(99)00193-1
- Smith, D., Spanel, P., and Mayhew, C. A. (1992). A selected ion-flow tube study of the reactions of O⁺, H⁺ and HeH⁺ with several molecular gases at 300 K. *Int. J. Mass Spectrom. Ion Proc.* 117, 457–473. doi: 10.1016/0168-1176(92)80108-d
- Sun, L. P., and Schatz, G. C. (2005). Direct dynamics classical trajectory simulations of the O⁺ + CH₄ reaction at hyperthermal energies. *J. Phys. Chem. B* 109, 8431–8438. doi: 10.1021/jp0454568
- Townsend, D., Miniti, M. P., and Suits, A. G. (2003). Direct current slice imaging. *Rev. Sci. Instrum.* 74, 2530–2539. doi: 10.1063/1.1544053
- Udseth, H., Giese, C. F., and Gentry, W. R. (1973). Transition probabilities and differential cross-sections for vibrational excitation in collisions of H⁺ with H₂, HD, and D₂. *Phys. Rev. A* 8, 2483–2493. doi: 10.1103/PhysRevA.8.2483
- Wakelam, V., Herbst, E., Loison, J. C., Smith, I. W. M., Chandrasekaran, V., Pavone, B., et al. (2012). A kinetic database for astrochemistry (KIDA). *Astrophys. J. Suppl. Ser.* 199. doi: 10.1088/0067-0049/199/1/21
- Wolfgang, R., and Cross, R. J. (1969). Intensity contour maps in molecular beam scattering experiments. *J. Phys. Chem.* 73, 743.
- Zabka, J., Farnik, M., Dolejšek, Z., Polach, J., and Herman, Z. (1995). Dynamics of the hydride ion transfer-reaction between CD₃⁺ and CH₄ - a crossed-beam scattering study. *J. Phys. Chem.* 99, 15595–15601.
- Zhang, J. X., Mikosch, J., Trippel, S., Otto, R., Weidemüller, M., Wester, R., et al. (2010). F⁻ + CH₃I → FCH₃ + I⁻ Reaction dynamics. Nontraditional atomistic mechanisms and formation of a hydrogen-bonded complex. *J. Phys. Chem. Lett.* 1, 2747–2752. doi: 10.1021/jz1010658

AUTHOR CONTRIBUTIONS

LP conducted the experiment reported here, analyzed the data, and produced the figures. JF suggested the problem and wrote up the initial draft of the presentation of the results. LP and JF discussed the analysis and interpretation of the experimental results together.

ACKNOWLEDGMENTS

The authors acknowledge support for this work under National Science Foundation grants CHE-1012303 and CHE-1265406.